Fast mechanical synthesis, structure evolution, and thermal stability of nanostructured CoCrFeNiCu high entropy alloy

N.F. Shkodich, I.D. Kovalev, K.V. Kuskov, D.Yu. Kovalev, Yu.S. Vergunova, Yu.B. Scheck, S.G. Vadchenko, O. Politano, Florence Baras, A.S. Rogachev

HAL Id: hal-03482861

https://hal.science/hal-03482861

Submitted on 16 Dec 2021

Fast mechanical synthesis, structure evolution, and thermal stability of nanostructured CoCrFeNiCu high entropy alloy

N.F. Shkodich[a,b*]**, I.D. Kovalev**[a]**, K.V. Kuskov**[b]**, D.Yu. Kovalev**[a]**, Yu.S. Vergunova**[a]**, Yu.B. Scheck**[a]**, S.G. Vadchenko**[a]**, O. Politano**[c]**, F. Baras**[c]**, A.S. Rogachev**[a,b]

[a]Merzhanov Institute of Structural Macrokinetics and Materials Science, Russian Academy of Sciences, Chernogolovka, Moscow, 142432 Russia
[b]Center of Functional Nano-Ceramics, National University of Science and Technology MISIS, Moscow, 119049 Russia
[c]ICB laboratory, UMR 6303 CNRS-Université Bourgogne Franche-Comté, 9 Av. Alain Savary, BP 47870, 21078 Dijon Cedex, France

* Correspondence: n.f.shkodich@mail.ru

Abstract:

A powder of equiatomic CoCrFeNiCu high entropy alloy (HEA) was prepared by short-term (120 min) high energy ball milling (HEBM). Our structural and chemical analysis showed that microsized particles of *fcc* CoCrFeNiCu with a grain size of 8 nm were obtained after 120 min of HEBM at 694/1388 rpm. The structural/phase evolution of CoCrFeNiCu HEA powder and its thermal stability were explored by high-temperature XRD at 600 °C, 800 °C and 1000 °C, by DSC up to 1500 °C, through the consolidation by SPS at 800 °C and 1000 °C, and characterized using XRD, SEM and EDX analyses. In-situ HT XRD analysis during 5.5 h of annealing showed the involvement of transient phases: the *bcc* phase that appeared in 1 h of annealing at 600 °C and disappeared at higher temperatures; and the fcc^1 phase (Cu-rich) arising in 2 h of annealing at 800 °C and disappearing at 1000 °C in 3 h of annealing. SPS consolidation at 1000 °C and annealing at 1000 °C for 5.5 h were found to result in the formation of single-phase fcc^2 CoCrFeNiCu alloy with a lean amount of Cu. The melting points for Cu-rich and Cu-depleted HEAs were found as 1118 °C and 1288 °C (Calphad calculations) and 1115 °C and 1365 °C (DSC measurements), respectively. SPS consolidation at 1000 °C under a pressure of 50 MPa yielded the single-phase *fcc* $CoCrFeNiCu_{0.5}$ alloy that turned thermodynamically more favorable than the equiatomic one. Thus, we can suppose thereupon, that the equiatomic *fcc* phase that appears after 120 min of HEBM is metastable because of the excess of Cu atoms. During annealing in the temperature range 800–1000 °C, the Cu-rich fcc^1 phase precipitates from the initial single-phase alloy, while the "mother phase" transforms into the more stable Cu-depleted fcc^2 phase. The chemical compositions of Cu-depleted and Cu-rich phases for the SPS-consolidated HEA CoCrFeNiCu alloy (at 800 °C) were determined from TEM–EDX analyses. Optimal combination of short-term HEBM and SPS consolidation can be recommended as a facile route to fabrication of single-phase *fcc* equiatomic CoCrFeNiCu HEA powders and bulk materials with good structural/elemental homogeneity.

Keywords: thermal stability, high energy ball milling, high entropy alloy, spark plasma sintering, *fcc* structure, Calphad approach

1. Introduction

As is known, material properties play a major role in many fields of applications and they always depend on structure. The ability of retaining these properties depends on the structural stability in different environments such as corrosive media, high/low temperature, high load/high speed and other extreme conditions. High entropy alloys (HEAs) show excellent properties in some respects, such as high strength and corrosion resistance, outstanding mechanical properties including yield strength, creep properties, fracture toughness, and promising magnetic properties [1–6].

The HEAs concept has been proposed by Yeh et al. in 2004 [7]. In the same year, Prof. Cantor independently suggested a similar concept to design multicomponent alloys (MCAs) [8]. The authors have established that the HEAs (or MCAs) are the alloys that consist of five or more principal elements whose volume fractions is within the range of 5–35%. HEAs tend to exhibit the formation of simple solid solution structure—body-centered cubic (*bcc*), face-centered cubic (*fcc*), hexagonal closed packed (*hcp*) or their combinations—instead of intermetallic phases, stabilized due to a high configurational entropy of their mixing [7–9]. This discovery gave impetus to extensive studies in the field all over the world.

The basic assumption underlying the solid solution formation of HEAs first postulated by Yeh et al. [7], was consisted in the fact that the major factor of solid solution formation in HEAs is a configurational entropy (ΔS_{config}) of alloy, which is increased with increasing number of alloying elements (at least 5 or more, $\Delta S_{config} \geq 1.61R$, where R is the universal gas constant) in equatomic concentrations and thus intermetallic phases could be suppressed. This concept can be explained by considering the equation for Gibbs free energy.

Due to sufficiently large entropy (provided by the ΔS_{config}) the Gibbs free energy ΔG may turn negative. It means that a new phase can be stabilized. It is also possible to get negative ΔG even if mixing enthalpy (ΔH_{mix}) is positive. However, over the last decade it has become apparent that this prediction often fails [10–12].

Later, many other parameters have been proposed as the means for predicting the formation of solid solutions and phases in HEAs—such as mixing enthalpy (ΔH_{mix}) within specified range -11.6 kJ/mol $< \Delta H_{mix} < 3.2$ kJ/mol, atomic size difference (δ) within the accepted limits $0 \leq \Delta r \leq 6.5$ %, electronegativity ($\Delta \chi$), whose value should very small [13], and average valence electron concentration (VEC) (the *bcc* and *fcc* phases are formed for VEC < 6.87 and VEC ≥ 8.0, respectively; while *bcc* + *fcc* mixture coexist when $6.87 \leq$ VEC ≤ 8.0) [9].

To predict the formation of solid solutions in HEAs, parameters of VEC, Δr and $\Delta \chi$ were calculated (according to [9]) for the CoCrFeNiCu alloy and summarized in Table 1.

Table 1 Calculated parameters VEC, Δr and $\Delta \chi$ for CoCrFeNiCu alloy

Composition	ΔS_{mix}	VEC	Phase predicted	Δr, %	$\Delta \chi$
CoCrFeNiCu	$1.61R$	8.8	*fcc*	1.03	0.09

For the CoCrFeNiCu composition, the atomic size difference ($\Delta r = 1.03\%$) is well within the adopted limits $0 \leq \Delta r \leq 6.5$ % for solid solution formation. VEC $= 8.8$ falls into the range for the formation of a *fcc* solid solution (VEC ≥ 8) [14]. The electronegativity (EN) difference is 0.09. As is known [13], electronegativity $\Delta \chi$ has little or no influence on the formation of solid solution or amorphous phase. Even when no range has been prescribed for the formation of disordered solid solution, it was noted [15] that a larger value of $\Delta \chi$ is expected to aid the formation of a compound.

Besides promising properties of HEAs caused by their multiphase microstructure, the most important parameter for their potential applications is their thermal stability. It has been found that the phase evolution during heat treatment largely depends on such factors as alloy composition, concentration of the elements, and synthesis route [16–20].

Several synthesis routes to prepare HEAs have been suggested [9,19]. However, the most of HEAs are produced through melting routes [9]. A common drawback of this route is an inhomogeneous microstructure of solidified product. In order to get homogeneous HEAs, they should be annealed at elevated temperature and quenched.

One of the most promising techniques to produce homogeneous HEAs is mechanical alloying (MA). Through MA, almost any kind of homogeneous material can be produced at room temperature, thus avoiding segregation and product inhomogeneity [21–23].

MA also takes advantage of solubility even in case of immiscible systems [24] due to the enhanced diffusion rates in case of sub-micron powder blends. Since the first reports on a nanocrystalline AlCrCuFeTiZn alloy in 2008 [23], several nanocrystalline HEAs have been synthesized by mechanically alloying. The most of the solid solution phases in HEAs were formed within 15–40 h of conventional milling [19]. Such prolonged milling hours often result in the formation of amorphous HEAs. For example, complete amorphization of AlBCFeNiSi and AlBCeFeNiSi alloys was observed in 140 h and 240 h of milling, respectively [25]. A drawback of conventional MA is a long milling time, a low energy input and increased amount of contaminations from milling balls/jars (Fe, WC, etc.) This can be overcome by using short-term high energy ball milling (HEBM). Later, good densification characteristics and high hardness were observed for the HEAs synthesized by combined use of HEBM and spark plasma sintering (SPS) [19,26].

Among HEAs, CoCrFeNiCu composition has been extensively studied earlier as HEA thin films and coatings deposited by magnetron sputtering [27,28], as volume HEA materials (mechanically alloyed powders and consolidated bulk samples) [29–33]. Different amounts of Ti and Al are usually added to study the phase evolution, mechanical and magnetic properties of designed systems [16,17].

An *et al.* [27] reported the formation of the *fcc* single-phase HEA CoCrFeNiCu thin films with (111) preferential orientation along the film growth direction by magnetron sputtering. Their structure differed from that of as-cast bulk CoCrFeNiCu alloy used as a target; it was composed of two *fcc* phases, Cu-rich and Cu-depleted ones. Arfaoui *et al.* [28] studied the sputtered single-phase *fcc* CoCrFeNiCu in thin films by in-situ TEM annealing. The structural and morphological stability of single-phase *fcc* HEA thin film was found stable up to 400°C. Starting from 450 °C a *bcc* phase without any changes in morphology was observed.
This type of transformation was referred to as the diffusionless process [28]. Further increase in temperature leads to structural and morphological changes controlled by volume diffusion processes. Above 550 °C, the authors observed the formation of a new intermetallic *bcc* phase containing mainly Cr.

The most of studied CoCrFeNiCu-based alloys were synthesized by arc melting followed by quenching [29–31]. Only a few studies (mostly controversial) on the structure and stability of mechanically alloyed CoCrFeNiCu HEAs have been reported so far [32–34].

Praveen *et al.* [33] obtained nanostructured CoCrFeNiCu alloy with *fcc* (as a main phase) and *bcc* (minor) structures after 15 h of ball milling in a Fritsch Pulverisette-P5 mill. The SPS consolidation at 900 °C led to the formation of two *fcc* and σ phases in the bulk material. Based on SEM/EDX studies [33], it was concluded that one of the two *fcc* phases corresponds to a Cr-rich one while another, to a Cr-depleted one. The σ phase detected by XRD was not clearly visible in SEM.

Thangaraju *et al.* [34] studied the phase stability of mechanically alloyed single-phase *fcc* CoCrFeNiCu HEAs obtained after 5 h and 50 h of milling at 350 rpm and 200 rpm, respectively in a Fritzsch Pulverisette 4 planetary mill. Annealing of a single-phase *fcc* mechanically alloyed CoCrFeNiCu powder (5h at 350 rpm) showed its stability up to 800 °C; at higher temperatures, it decomposed into two *fcc* phases, one of them being Cu-enriched. At 1000 °C, the Cr precipitated out of the matrix.

The CoCrFeNiCu HEA prepared by MA for 65 h [32] represented a mixture of *bcc* (as a main phase) and *fcc* (minor) phases. Results of in-situ high temperature X-ray diffraction (HT XRD) have shown low thermal stability of HEA powders (up to 350 °C) due to diffusion-assisted transformation into precipitates of the σ phase. Eventually, annealing at 800 °C for 2 h led to the formation of the simple *fcc* phase with a negligibly low admixture of the σ phase [32].

In view of the inconsistency between the available data [32–34] on the structure/phase formation and thermal stability in mechanically alloyed CoCrFeNiCu HEAs, in this communication we report on the fast synthesis of equiatomic CoCrFeNiCu high entropy alloy by high energy ball milling and its structural characterization and phase evolution by X-ray

diffraction (XRD), scanning electron microscopy (SEM) and energy dispersive X-Ray (EDX). The structural/phase evolution and thermal stability of HEBM CoCrFeNiCu HEA powders were studied by in-situ HT XRD, differential scanning calorimetry (DSC) and through SPS consolidation. Phase fractions and phase composition as a function of temperature were calculated by Calphad methodology with the TCHEA3 database (Thermo-Calc®).

2. Experimental

Commercial powders of Co (99.7% pure, mean particle size 3 µm), Cr (99.35%, >71 µm), Fe (99.96%, 10–20 µm), Ni (99.5%, 45–60 µm), and Cu (99.5%, 45–60 µm) were used as starting materials.

HEBM of equiatomic CoCrFeNiCu HEA powder mixtures was performed in a water-cooled planetary ball mill Activator-2S using stainless steel cylindrical jars and balls (7 mm in diameter). In all cases, the ball/powder weight ratio was 20 : 1. The vial was evacuated and then filled with Ar gas at 4 bar. The HEBM was run at a rotating speed of the sun disk and the grinding drums at 694 and 1388 rpm, respectively. Milling time (t) was varied between 30 and 120 min.

`As-prepared and milled CoCrFeNiCu powders were SPS-consolidated in vacuum in a Labox 650 facility (Sinter Land, Japan). The powder mixture was placed into a cylindrical graphite die (inner diameter 12.7 mm) and uniaxially compressed at 50 MPa. The sample was heated at a rate of 100°C/min up to some preset sintering temperature in the range 800–1000 °C by passing rectangular pulses of electric current through the sample. The dwell time at sintering temperature was 10 min. SPS-produced disks were 2–3 mm thick and 12.7 mm in diameter.

Microstructure, crystal structure, and local composition of initial, milled, and consolidated powders were characterized by XRD (DRON-3M diffractometer, Fe-K_α radiation, 2θ =40–120°), SEM (Zeiss Ultra+, Carl Zeiss, Germany), and EDX (Oxford Inca spectrometer and Aztec software).

For TEM analysis, the lamellas of CoCuFeNiCu HEA powder particle and HEA bulk sample were prepared by a focused ion beam technique using a Nanolab 6000 Helios Dual SEM/FIB (FEI, USA). The fine structure studies and compositional analyses were performed by using a Jeol JEM 2100 microscope (Japan) equipped with Oxford X-Max 80 EDX detector (UK).

Thermal stability of the HEA powders was studied by DSC (STA 449 F1 Simultaneous Thermal Analyzer, Netzsch, Germany, up to 1500°C, heating rate 20°C/min, in an Ar atmosphere), and HT XRD.

High-temperature XRD measurements were made in situ in vacuum (10^{-3} Pa) using an ARL`XTRA`diffractometer (Thermo Fisher Scientific, USA) equipped with a high-temperature chamber HTK2000 (Anton Paar, Austria). A layer of mechanically alloyed powder about 100 µm thick was placed on a surface of a flat tungsten heater and warmed-up at a rate of 300 deg/min up some pre-determined annealing temperature, i.e. 600 °C, 800 °C or 1000 °C. The annealing temperature was kept constant by means of an A1-type thermocouple and Eurotherm 2604 controller (Schneider Electric, England). Each sample was exposed to a constant annealing temperature during 5.5 h, with simultaneous permanent registration of XRD patterns in the range 2θ = 41–53° (Cu-K_α radiation). Sequences of high-temperature XRD patterns taken at different annealing time were used to trace the dynamics of crystal structure transformations in situ. After annealing and cooling down to room temperature, precise XRD analysis was made in the range 2θ = 20–140° in order to determine crystal cell parameters. Fitting the XRD peaks was made using NPP Burevestnik software based on pseudo-Voigt function. Phases were identified using Crystallographica Search-Match software and ICDD PDF2 database.

Thermodynamic calculations were performed using Thermo-Calc® software based on the Calphad methodology with the TCHEA3 database. Phase fractions and phase composition as a function of temperature were calculated for the equiatomic CoCrFeNiCu system.

3. Results

3.1 Phase Evolution during HEBM

Figure 1 represents XRD diffraction patterns of the CoCrFeNiCu powder mixtures ball-milled for different t. The non-milled blend exhibits expectedly strong and narrow Bragg peaks due to crystalline structure of the elements. With increasing t up to 15 min, a gradual broadening and partial overlapping of diffraction peaks was accompanied by a decrease in their intensity. Further increase in milling time t up to 30 min leads to a formation of the *fcc* ($a = 3.589 \pm 0.005$ Å) solid solution with the (110), (200), (220) peaks as a main phase with a minor admixture of the *bcc* ($a = 2.887 \pm 0.003$ Å) phase as evidenced by the (111) and (200) peaks. No further changes occur in the diffraction pattern for $t = 30$–90 min corresponding to the formation of two-phase structures. At $t = 120$ min, the diffraction pattern shows only the single solid solution with an *fcc* crystal structure ($a = 3.597 \pm 0.005$ Å).

Hence, the mechanical deformations caused by HEBM give rise to the transformation of initially microcrystalline powders to nanocrystalline solid solutions with the partially disordered crystal structure.
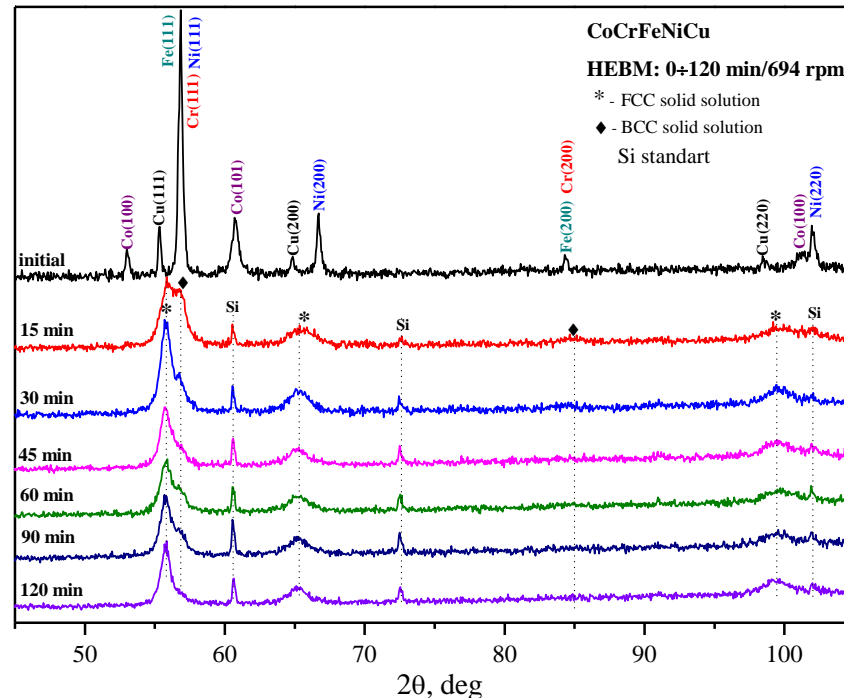

Fig. 1. XRD patterns of CoCrFeNiCu powder mixtures taken after HEBM for different t (indicated at the left). The patterns are shifted along the y axis for the sake of clarity.

The effect of milling time (t) on the crystallite size and strain in CoCrFeNiCu blends was derived from line broadening analysis. The pseudo-Voigt function as a convolution of a Gaussian and a Lorentzian component (the width of the Lorentzian component is related to the grain size while the Gaussian width, to the lattice strain) was used for fitting XRD peak profile and Si standard was used to correct instrumental broadening. Crystallite size, lattice strain for *fcc* phase were calculated using the Williams–Hall method [35].

For the non-milled CoCrFeNiCu powder blends, the crystallite size of each element exceeds 300 nm. An increase in duration t of HEBM gave rise to a decrease in the size of crystallites for both individual elements (up to 15 min) and binary/ternary solid solutions such as CuNi, FeNi, FeNiCo, etc. ($t = 45$–120 min). In this case, lattice strains grew over this period. The crystallite size and lattice strain for single-phase *fcc* CoCrFeNiCu solid solution formed in 120 min of HEBM were found to have a value of 8 nm and 0.7%, respectively

The phase transformation of CoCrFeNiCu powder as a function of milling time was also studied by SEM/EDX. During the initial HEBM stage ($t = 30$ min), randomly distributed particles of initial elements transformed into a layered structure that is typical for ductile metal blends processed in a planetary ball mill (Fig. 2a). Further mechanical treatment ($t = 60$ min) leads to decrease of the average layer thickness, also homogenized areas were detected (Fig. 2b).

At $t = 120$ min the layer structure vanished completely and a relatively uniform distribution of initial elements was observed (Fig. 2c).
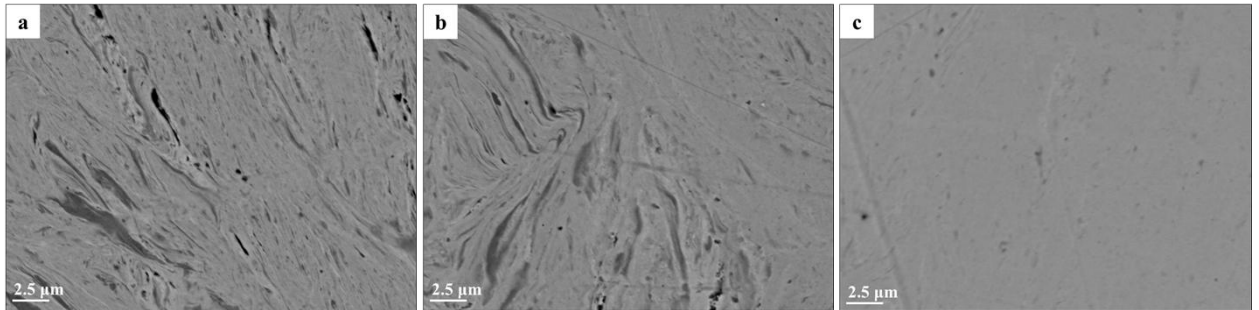

Fig. 2. SEM images (cross-section) of CoCrFeNiCu powder blends after HEBM (694/1388 rpm) for $t = 30$ (a), 60 (b), and 120 min (c).

The SEM/EDX results for CoCrFeNiCu powder particles milled for $t = 120$ min (Fig. 3) show that the elements Co, Cr, Fe, Ni, and Cu are uniformly distributed on a micro-scale level, on retention of starting elemental composition (at. %): Cu 20.2, Cr 19.9, Fe 20.3, Ni 19.9, and Co 19.7.
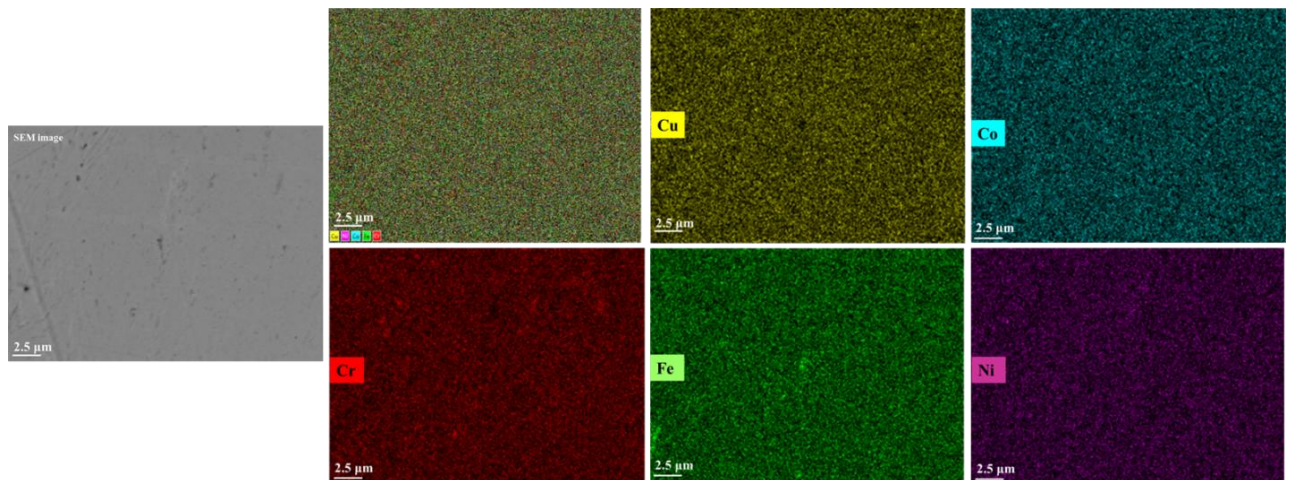

Fig. 3. SEM image and EDX-mapping for the cross-section of powder CoCrFeNiCu particle after HEBM ($t = 120$ min).

At this step, we may conclude that the formation of HEA powder particles with the single *fcc* structure ($a = 3.597 \pm 0.005$ Å) is reached after HEBM for $t = 120$ min (at 694/1388 rpm).

TEM analysis of the CoCeFeNiCu HEA powder obtained after 120 minutes of HEBM, has shown a nanocrystalline structure (Fig. 4a) and uniform distribution of the elements on an atomic scale (Cu 20.78, Cr 20.13, Fe 19.73, Ni 19.69, and Co 19.67.) (Fig. 4b). According to the phase analysis of the electron diffraction pattern (Fig 4a, insert) *fcc* phase reflections were identified, which is in good agreement with the XRD data.
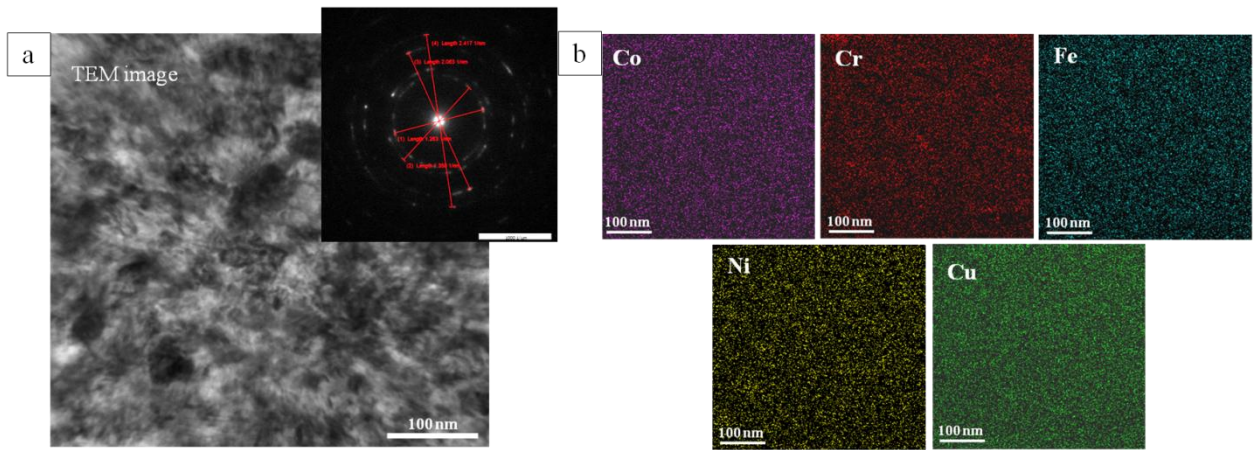
Fig. 4. (a) BF TEM image and selected area electron diffraction (SAED) pattern of 1μm area and (b) STEM EDX mapping of CoCrFeNiCu HEA powder produced after 120 min of HEBM.

3.2 Thermal Stability of CoCrFeNiCu HEA powder as studied by HT-XRD

In-situ HT XRD measurements during 5.5 h at constant annealing temperature (600 °C, 800 °C or 1000 °C) were conducted for the single phase *fcc* CoCrFeNiCu HEA powder prepared by HEBM for t = 120 min.

After 1 h of exposure during annealing at 600 °C, a small amount of the *bcc* (110) phase is seen (Fig. 5) to appear and grow with increasing holding time (up to 5.5 h). During annealing we did not notice any significant changes in broadening and intensity of diffraction peaks. There was only a diffraction line shifting to the smaller angles associated with thermal expansion. After cooling down, the material was found to contain the *fcc* phase as a main one (a = 3.581 ± 0.002 Å) and small admixture of the *bcc* phase.
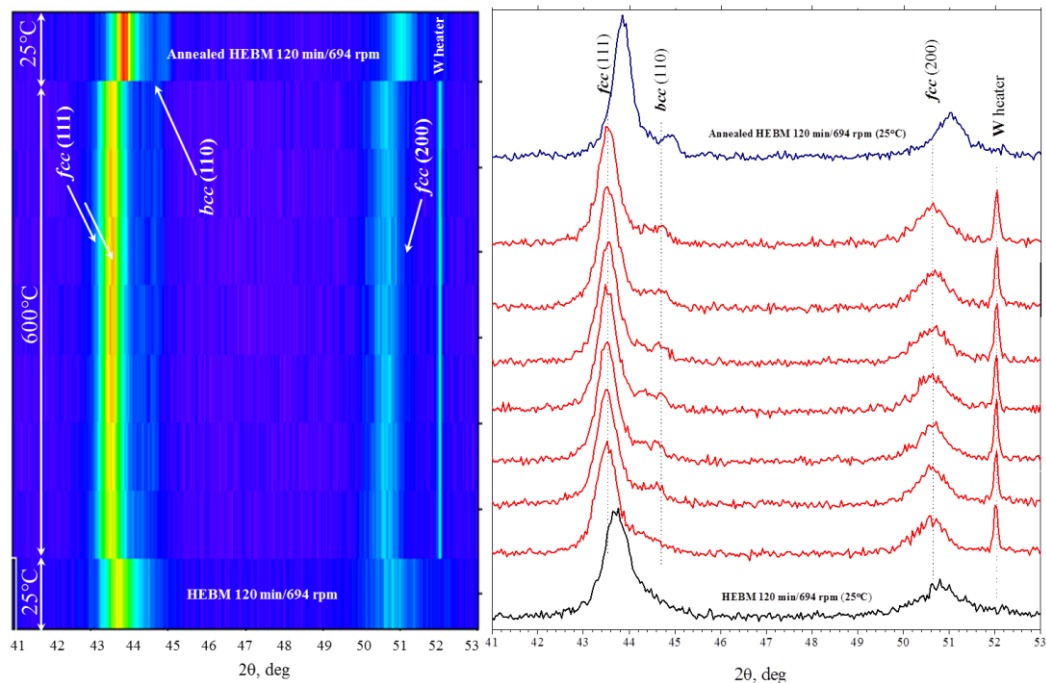

Fig. 5. High-temperature diffraction patterns for HEA CoCrFeNiCu powder (t = 120 min) at 600ºC.

During annealing at 800 °C (Fig. 6), we did not observe the formation of the *bcc* phase detected at 600 °C earlier. It is known that in iron-based alloys with a *bcc* structure at room temperature, heating to 700–800 °C induces a polymorphic *bcc* (*Im-3m*)–*fcc* (*Fm-3m*)

transformation. Holding HEA powders at 800°C leads to partial decomposition of the *fcc* phase into two *fcc* structures (fcc^1 $a = 3.608 \pm 0.002$ Å; fcc^2 $a = 3.572 \pm 0.002$ Å). Note that the fcc^1 phase appears at 800 °C after 2 h of annealing.
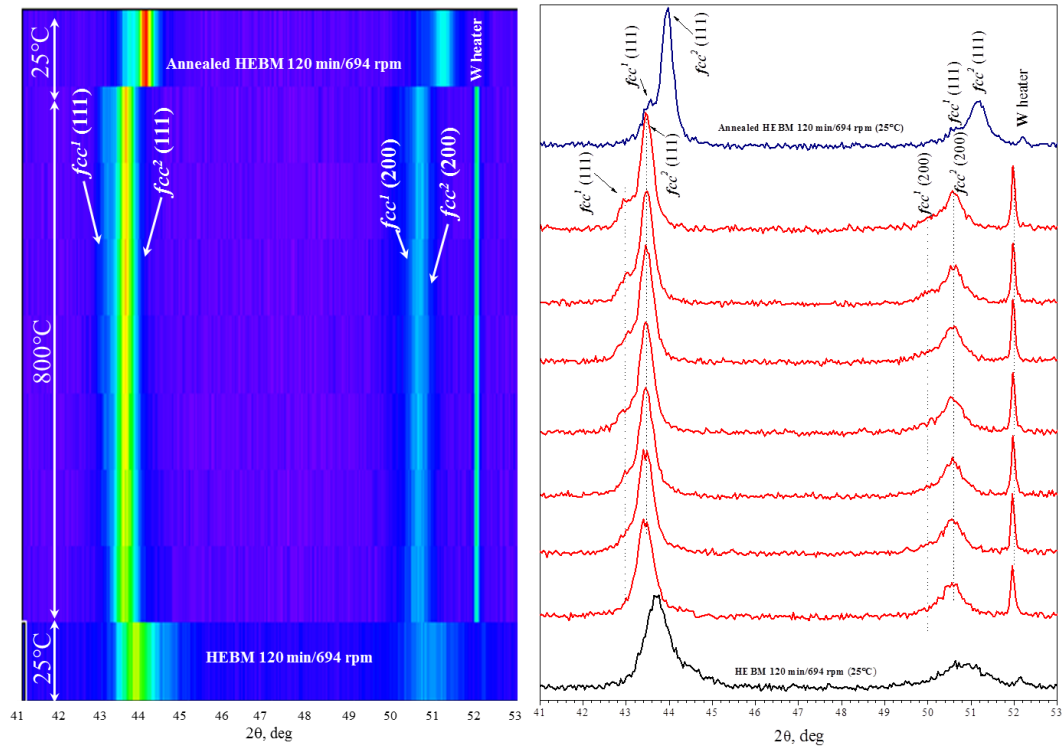

Fig. 6. High-temperature diffraction patterns for HEA CoCrFeNiCu powder ($t = 120$ min) at 800 °C.

Annealing at 1000 °C for 5.5 h promotes a decrease of the crystallinity of the fcc^1 phase and, after 2 h of holding, this phase could not be clearly detected any more by XRD (Fig. 7a). The high-temperature annealing gives rise to the formation of single-phase with a fcc^2 structure ($a = 3.572 \pm 0.002$ Å) whose amount grows with increasing dwell time due to annealing of structural defects formed during HEBM. The final product is seen to contain a single-phase fcc^2 structure after cooling down. However, in SEM images (Fig. 7b) the material is composed of two phases. One corresponds to the pure Cu segregating mostly on the surface of powder particles, also as evenly distributed thin layers inside the particles. Another is a single *fcc* solid solution depleted in Cu. We did not observe the splitting of two phases in XRD patterns, most likely because of very small difference in lattice parameters of *fcc* solid solutions which could not be discerned by conventional XRD. Also, content of the surface-segregated Cu-rich phase can be too small to be detected by XRD analysis.
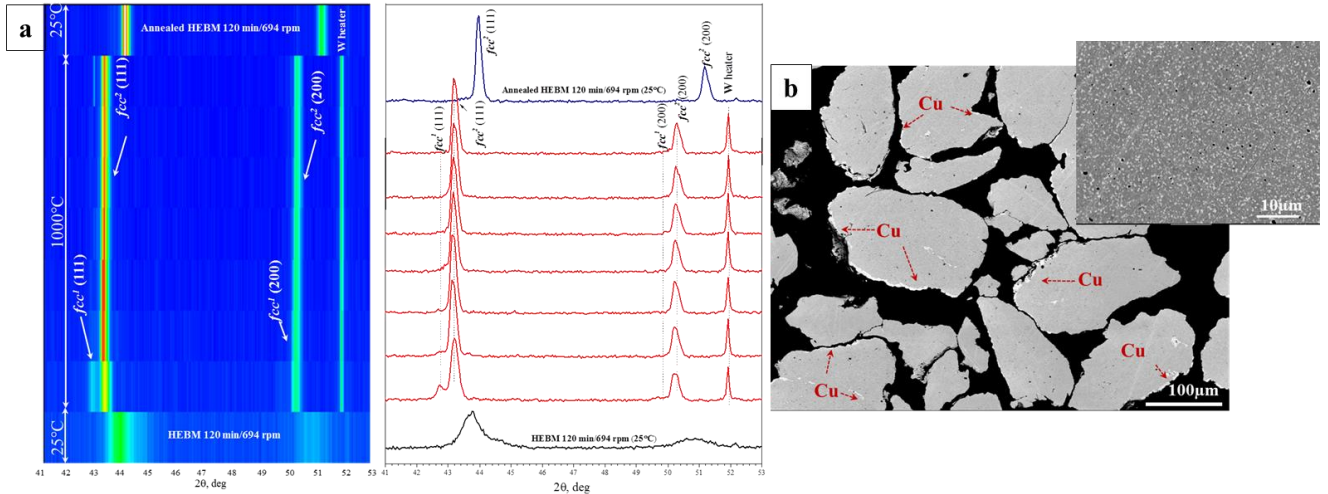
Fig. 7. (a) High-temperature diffraction patterns at 1000 °C and (b) SEM images taken after cooling down for HEA CoCrFeNiCu powder (*t* = 120 min)

3.3 Thermal stability of CoCrFeNiCu HEA powder as studied by DSC

Thermal stability of HEA CoCrFeNiCu powder (*t* = 120 min) and powder blend of starting elements (for comparison) was investigated through dynamic DSC in Ar up to 1500 °C (Fig. 8). The DSC curve 1 (black) of initial powder blend exhibits two major endothermic peaks around 1083 °C and 1397 °C. The endothermic peak at 1083 °C (heat of fusion −8.6 J/g) corresponds to the Cu melting (T_m = 1083 °C), while the second peak at 1359 °C with heat of fusion −62.5 J/g, to the melting of entire CoCrFeNiCu composition.

DSC curve *2* (red) was obtained for CoCrFeNiCu HEA powder. The first low and very wide exothermic peak in the temperature range 405–623 °C (peak maximum at 551 °C) is associated with the release of internal stresses arising from structural deformation, lattice strain, etc. The other shallow endothermic peak (in the range 847–1047 °C) is related to energy absorption processes. Comparing obtained DSC results with HT XRD data we can assume that this endothermic peak is due to a decomposition of single *fcc* phase into fcc^1 and fcc^2 phases. The two falls of the heating curve *2* after 1107 °C (peak maximum at 1115 °C) and after 1328 °C (peak maximum at 1365 °C) indicate the melting of two phases, most likely one is the Cu-rich (close to the melting temperature of a pure Cu) while the other, Cu-depleted HEA alloy composition, respectively.
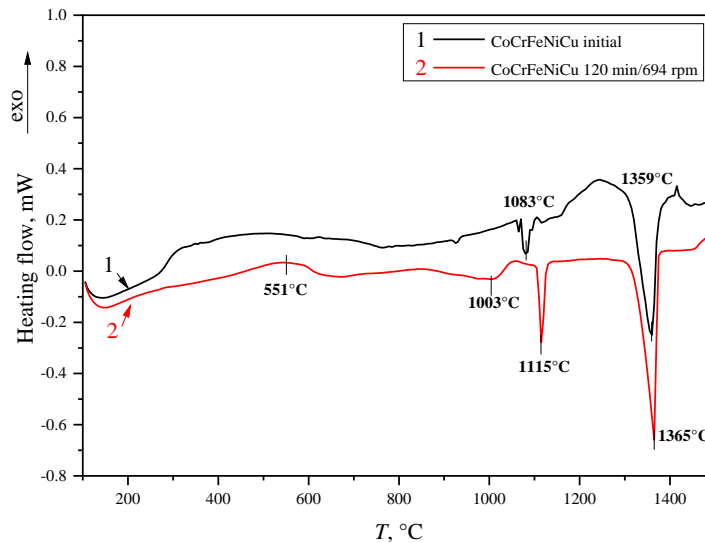

Fig. 8. DSC curves for CoCrFeNiCu powders: (1) initial and (2) after 120-min HEBM.

3.4 Thermal Stability of CoCrFeNiCu HEA powder during SPS consolidation

The thermal stability of the CoCrFeNiCu HEA powder was also studied in the condition of bulk material formation by using SPS. The CoCrFeNiCu non-milled and HEA (t = 120 min) powder blends were SPS consolidated at 800 °C and 1000 °C. As evidenced by our XRD results, the SPS of starting powder blend at 800 °C results in peaks broadening and their partial overlapping at 56.42° (Fig. 9, red line spectra). The diffraction peaks of individual elements are still present on XRD spectra. On SEM-BSE image (Fig.10a), where the contrast is defined by the atomic number of a given element or phase (contrast is Z-sensitive), the Cu-rich areas (Z = 29) look lighter than the other elements: Cr (Z = 24), Co (Z = 27), Fe (Z = 26), Ni (Z = 28).

The distribution of principal elements is shown in color-scale contours determined by EDX (Fig. 10a). During SPS (when pulses of electric current passed through the sample) the temperature inside of the sample may exceed the temperature of the graphite die by more than 100 °C. Thus, the pre-alloying of elements was observed due to partial material melting at grain boundaries.

An increase in sintering temperature up to 1000 ºC leads to the formation of the *bcc* and *fcc* solid solutions (Fig. 9, blue line spectra). But some negligible peaks of individual elements are still present on XRD data. SEM and EDX analyses (Fig. 10b) have shown that the dissolution of metals grows with an increase of sintering temperature. However, the material looks like a multiphase one.
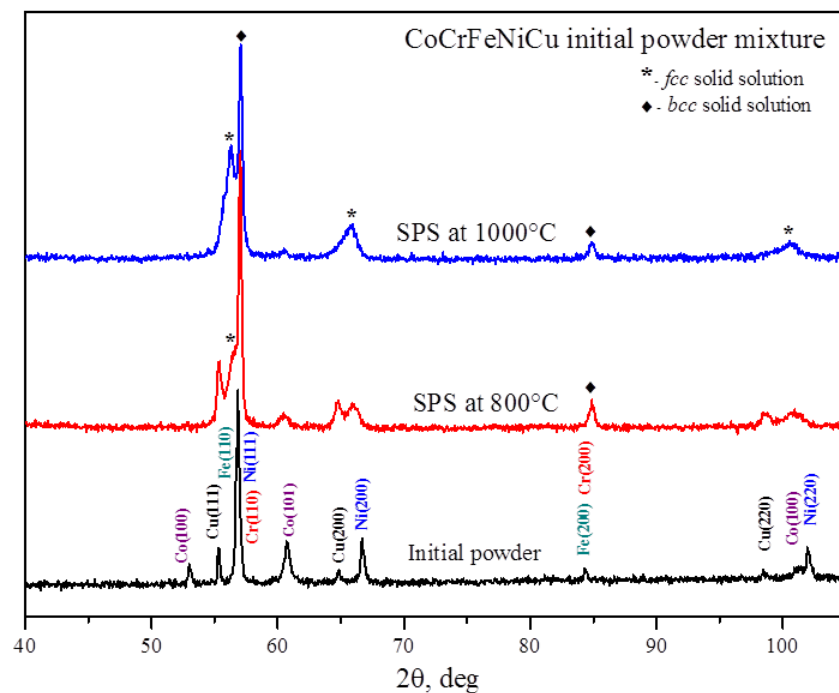

Fig. 9. XRD patterns of initial CoCrFeNiCu powder blend and CoCrFeNiCu bulk specimens sintered at different temperatures.
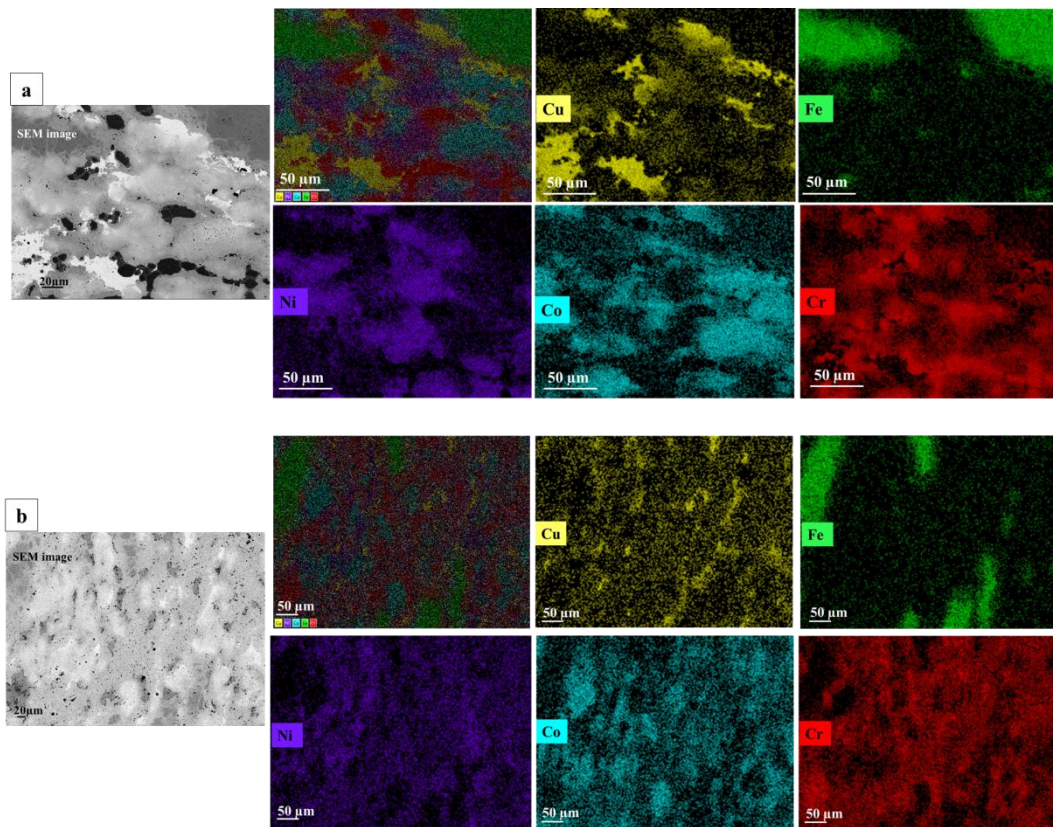
Fig. 10. SEM images and EDX-mapping of the cross-section of CoCrFeNiCu alloy sintered from initial powder blends by SPS: (a) at 800 °C and (b) at 1000 °C

The XRD analysis of the HEA CoCrFeNiCu powder blend after SPS at 800 ℃ illustrates the formation of two phases with a *fcc* structures (*fcc*[1]: a = 3.611 ± 0.001 Å; *fcc*[2]: a = 3.580 ± 0.001 Å) (Fig. 11, red line spectra). Based on SEM/EDX results suggest that the formation of the *fcc*[1] phase is caused by segregation of Cu that intensifies with an increase of sintering temperature up to 800 °C in the intergranular regions (Fig. 12a).

Further increase in the sintering temperature in combination with the applied pressure during SPS processing displaces the area of Cu segregation from the center to the edge and then out of the cylindrical sample through the graphite die (see in a supplementary file). As a result, a single-phase *fcc*[2] structure with Cu-depleted content in the sample (corresponds to CoCrFeNiCu$_{0.5}$ composition, see Fig. 10, blue line pattern, Fig.12b and Table 2) was obtained. It was observed [36] that an increase in the Cu content in CuNiCoZnAlTi HEA during annealing leads to an increase in the number *fcc* phases in a final product. In conditions of our SPS sintering, the single-phase *fcc* CoCrFeNiCu$_{0.5}$ HEA is energetically more preferable than the equiatomic CoCrFeNiCu composition.
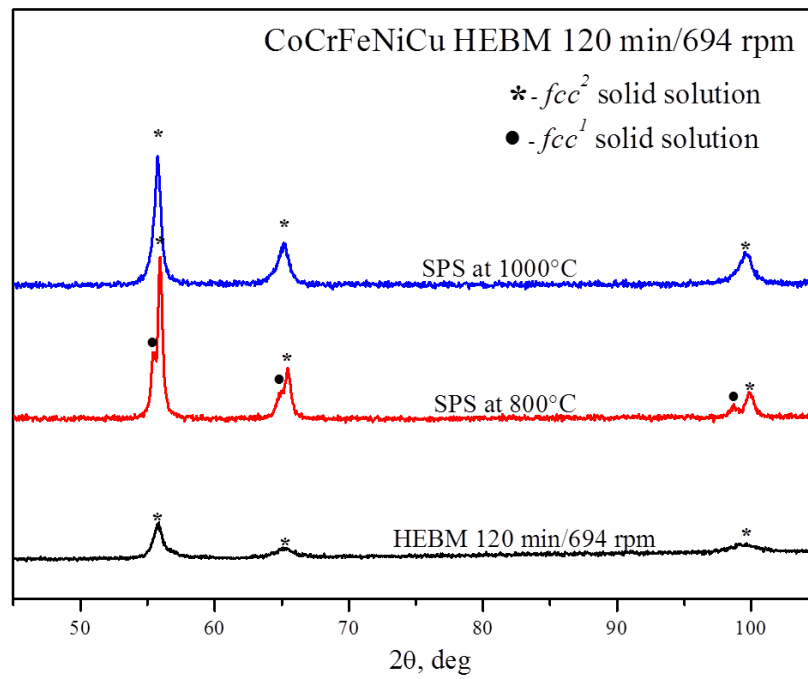
Fig. 11. XRD patterns of initial CoCrFeNiCu powder blend and CoCrFeNiCu bulk specimens sintered at different temperatures (indicated).
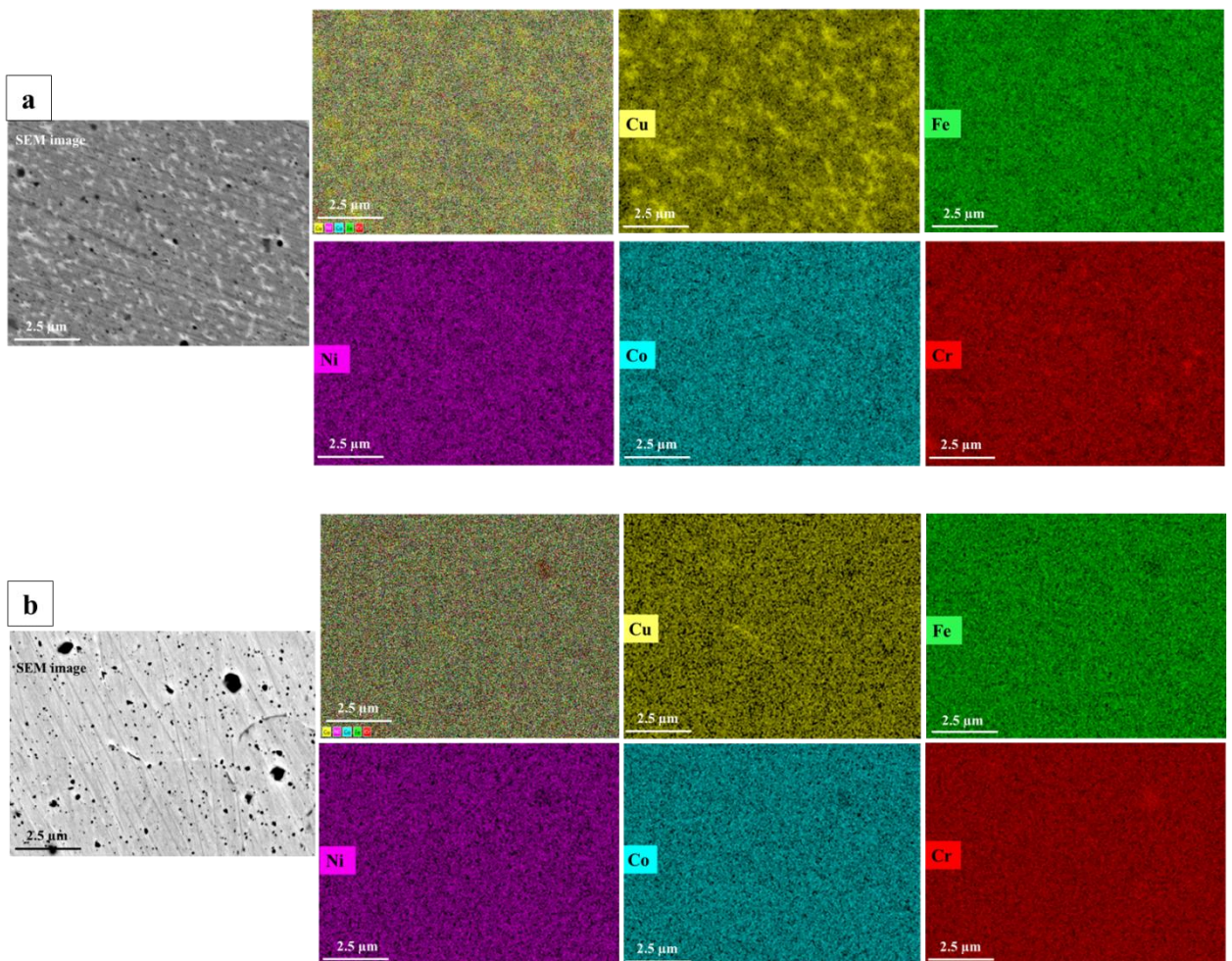

Fig. 12. SEM images and EDX-mapping of the cross-section of bulk CoCrFeNiCu HEA sintered from HEA powder blend by SPS: (a) at 800 °C and (b) at 1000 °C.

Table 2. Chemical composition (at. %) of the CoCrFeNiCu HEA powder SPS consolidated at 1000 °C

Composition	Preparation conditions	Composition (at.%) – EDX				
		Co	Cr	Fe	Ni	Cu
CoCrFeNiCu	HEBM: 120 min, 694/1388 rpm, (Ar) SPS: 1000 °C, 10 MPa, 10 min	22.6 ± 1.8	22.6 ± 1.6	23.7 ± 1.3	22.1 ± 0.9	9 ± 1.2

The detailed TEM investigation reveals that bulk CoCrFeNiCu HEA sample consolidated by SPS at 800 °C consists of the grains with a size of about fifty to several hundred nm (Fig. 13a). Concentration profiles of Co, Cr, Fe, Ni and Cu along the scan line determined by STEM-EDX implies that the material consists predominantly of the grains with two different elemental compositions: one is Cu-rich phase, while another looks like a Cu-depleted one (Fig. 13b).
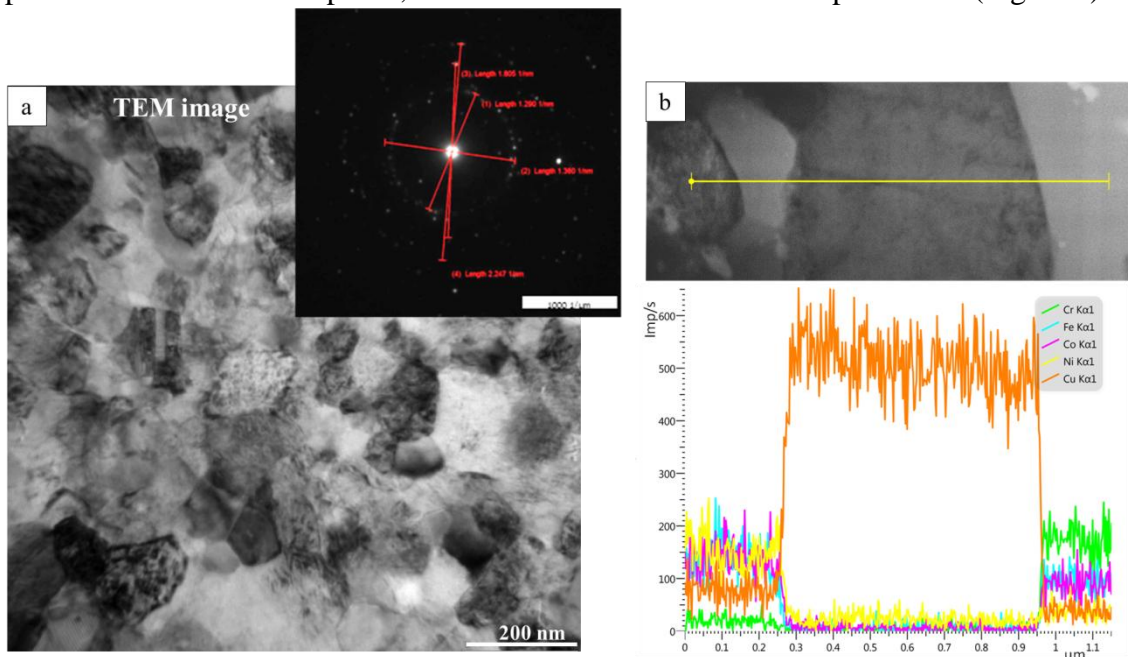

Fig. 13. (a) BF TEM image and electron diffraction (ED) pattern (insert) of 1 µm in diameter area and STEM EDX mapping (b) STEM image with a scan line and concentration profiles of Co, Cr, Fe, Ni and Cu along the line as determined by EDX of SPS-consolidated CoCrFeNiCu HEA sample.

Chemical composition of Cu-rich and Cu-depleted phases of SPS-consolidated (800 °C) CoCrFeNiCu HEA sample were determined by STEM-EDX at 10 points for each phase. The results are collected in Table 3.

Table 3. Chemical composition (at. %) of the CoCrFeNiCu HEA powder SPS consolidated at 800 °C as determined by EDX

Composition		Composition (at. %)				
		Co	Cr	Fe	Ni	Cu
CoCrFeNiCu	fcc^2 (Cu-depleted)	19.18 ± 0.94	38.11 ± 0.69	23.11±0.64	8.01±0.54	11.59±1.68
	fcc^1 (Cu-rich)	3.14±0.94	0	0.81 ±0.05	0.78 ±0.04	95.26 ± 0.81

Thermodynamic calculations for CoCrFeNiCu composition were performed using the Calphad method, those based on a free energy minimization, gives the dependence of the equilibrium phase composition on temperature. Phase fraction plot for CoCrFeNiCu is shown in Fig. 14a. Small amount of *bcc* and σ phases were calculated to present below 600 °C and 700 °C respectively. At higher temperatures ($T > 700$ °C) the coexistence of two disordered *fcc* solid solutions in CoCrFeNiCu HEA was predicted. One is the fcc^1 phase with a Cu predominance ($Co_{0.01}Fe_{0.02}Ni_{0.08}Cr_{0.004}Cu_{0.89}$, blue line in Fig .14a), while another is the fcc^2 solid solution characterized by a low amount of Cu ($Co_{0.25}Fe_{0.25}Ni_{0.23}Cr_{0.25}Cu_{0.02}$, red line in Fig.14a). The Cu-rich (fcc^1) and Cu-depleted phases (fcc^2) were found to melt at 1118 °C and the 1288 °C, respectively.

The lattice parameters of fcc^1 and fcc^2 phases as determined from in-situ HT XRD data at 800 °C and 1000 °C (excluding holding time) and calculated by Calphad at these temperatures have shown a good agreement. (Fig. 12 b).
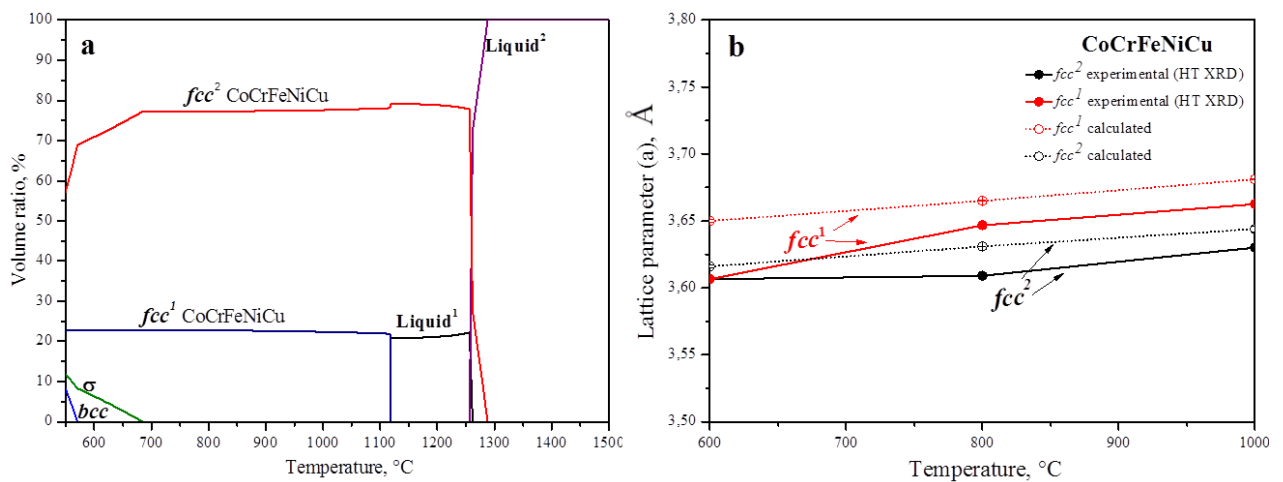

Fig. 14. (a) Calculated phase fraction plot of CoCrFeNiCu as a function of temperature and (b) comparison of calculated (shot-dot lines) and measured values of lattice parameters at different temperatures (indicated).

4. Discussion

The HEBM treatment of CoCrFeNiCu powder blend by HEBM for 120 min results in the formation of a single-phase alloy powder a with *fcc* structure (Fig. 1) with uniform distribution of principal elements (Figs. 2a and 3). The CoCrFeNiCu HEA powder with the same structure was achieved after 5 h (at 350 rpm) and 50 h (at 200 rpm) of ball milling [34]. However, the single phase *fcc* CoCeFeNiCu alloy had not been obtained [32] even after 65 h of mechanical treatment in a planetary ball mill at 200 rpm. The material consisted of *bcc* and *fcc* solid solutions.

Our results show that the process of phase formation in mechanically alloyed CoCrFeNiCu HEA strongly depends on the acceleration of the planetary ball mills. However, this is not a main parameter that defines the features of the process taking place during mechanical treatment. Many other parameters—such as (a) type and configuration of a mill; (b) material and size of milling bodies; (c) drum material; (f) mass of milling bodies; (g) ball/powder ratio; (i) ambient atmosphere of milling, etc.—affect the rate, effectiveness, and the extent of structural transformations during mechanical treatment.

Among other ball mills, the Activator 2S used in a present study, is of utmost energy intensity (maximal rotation rate, maximum centrifugal acceleration of the milling balls) as compared to such brands as Spex 8000 (Spex Certi Prep, Inc.), Pulverizette (Fritzsch), PM 400

(Retsch) etc. The amount of energy input into milled powder per time unite is defined by practically all the governing parameters, that is by a mill type. Since energy intensities of various mills differ by several orders of magnitude, so do the durations of mechanical treatment with these mills.

The in-situ HT XRD results for CoCrFeNiCu HEA powder (t = 120 min) at 600 °C have shown the appearance of small amount of bcc phase after 1 h of annealing, which is disappeared at higher temperatures. After 2 h of annealing at 800 °C, the single fcc phase decomposed into two fcc structures (fcc^1 a = 3.608 ± 0.002 Å; fcc^2 a = 3.572 ± 0.002 Å). They are still present at 1000 °C during 3 hours of annealing and transform again into a single fcc phase (a = 3.572 ± 0.002 Å), which remains stable after cooling down.

The bcc phase detected by in-situ HT XRD at 600 °C (Fig. 5) is predicted by Calphad at a lower temperature (Fig .14a). The same situation was observed in case of the fcc^2 phase, whose appearance was predicted by Calphad below 600 °C. Despite the recent trend in developing predictive parameters by Calphad approach, it depends on equilibrium thermodynamic database. However, the HEBM process is non-equilibrium.

On one hand, based on our thermodynamic calculations starting from the 700 °C and higher (up to T_{melt}) the material consisted of two fcc phases that melt at 1118 °C (Cu-rich) and 1288 °C (Cu-depleted), respectively. The calculated predicts have been confirmed experimentally by DSC. The presence of two phases with different melting temperatures (1115 °C and 1365 °C) was observed (Fig. 8).

On the other hand, in-situ HT XRD during long annealing (5.5 h) at 1000 °C and after sintering by SPS at 1000 °C results in the formation of the CoCrFeNiCu HEA with a Cu-depleted single fcc^2 phase. In case of HT XRD, the long temperature annealing leads to the grain growth and an increase a diffusion of atoms in lattice, and accordingly, the Cu segregates mostly on the surface of powder particles, also as evenly distributed thin layers inside the particles.

As for SPS, a nanocrystalline nature of mechanically alloyed powders is retained after SPS at 1000 °C due to specific features of this process (synthesis is due to pulses of electric current passing through the powder and a die, short holding time) compared to conventional sintering methods. Also, since many elements are present in this alloy in equiatomic proportion, it offers resistance to atomic diffusion. However, the pressure applied during SPS may produce significant influence on the formation of final phase. In our case, the Cu-rich phase was displaced from the cylindrical sample through the graphite die and the single fcc^2 phase corresponded to the CoCrFeNiCu$_{0.5}$ composition is formed in SPS conditions. The resulting phase turned out to be more thermodynamically stable than the equatomic one.

Thus, we can suppose thereupon, that the equiatomic fcc phase that appears after 120 min of HEBM is metastable because of the excess of Cu atoms. During annealing in the temperature range 800–1000 °C, the Cu-rich fcc^1 phase precipitates from the initial single-phase alloy, while the "mother phase" transforms into the more stable Cu-depleted fcc^2 phase.

Conclusion

Nanocrystalline CoCrFeNiCu HEA powders were successfully prepared by short-term high energy ball milling (HEBM). Their structural/phase evolution and thermal stability were studied by HT-XRD (at 600 °C, 800 °C and 1000 °C), by DSC (up to 1500 °C), and through the

consolidation by SPS (at 800 °C and 1000 °C). The HEBM-processed, annealed, and consolidated CoCrFeNiCu HEA powders were characterized by XRD, SEM, TEM and EDX.

The results are summarized as follows:

(1) An equiatomic nanocrystalline CoCrFeNiCu high entropy alloy powder with a single *fcc* structure ($a = 3.597 \pm 0.005$ Å) was successfully prepared by short-term (120 min) HEBM at 694/1388 rpm in Ar.

(2) In-situ HT XRD analysis during annealing for 5.5 h has revealed the formation of transient phases: the formation of *bcc* phase after 1 h of annealing at 600 °C and its disappearance at higher temperatures; the formation of fcc^1 phase (Cu-rich) after 2 h of annealing at 800°C and its disappearance at 1000 °C after 3 h of annealing.

(3) The Cu segregation in the intergranular regions and formation of two solid solutions with *fcc* structures (fcc^1 $a = 3.608 \pm 0.002$ Å, fcc^2 $a = 3.572 \pm 0.002$ Å) in HEA CoCrFeNiCu alloy powder at 800 °C by SPS is caused by positive values of enthalpy of mixing between Cu and other elements.

(4) The chemical compositions of Cu-depleted and Cu-rich phases for the SPS-consolidated HEA CoCrFeNiCu alloy (at 800 °C) were determined from TEM–EDX analyses.

(5) In-situ HT XRD results show that the annealing at 1000 °C for 5.5 h and SPS consolidation at 1000 °C result in the formation of the CoCrFeNiCu HEA alloy with a single fcc^2 Cu-depleted phase.

(6) The melting points for the Cu-rich and Cu-depleted HEAs were found to have the values of 1118 °C and 1288 °C, respectively, as calculated by Calphad approach and of 1115 °C and 1365 °C as a determined by DSC method.

(7) During SPS at 1000 °C under applied pressure of 50 MPa, the formation of the CoCrFeNiCu$_{0.5}$ HEA with *fcc* single phase is thermodynamically more favorable than the equiatomic one.

(8) Optimal combination of HEBM and SPS processes can be recommended as a facile route to fabrication of equiatomic CoCrFeNiCu HEA powders and bulk materials with the best structural/elemental homogeneity.

Acknowledgment

References

[1]   Z. Li, K.G. Pradeep, Y. Deng, D. Raabe, C.C. Tasan, Metastable high-entropy dual-phase alloys overcome the strength-ductility trade-off, Nature. 534 (2016). https://doi.org/10.1038/nature17981.

[2]   M.C. Gao, P.K. Liaw, J.W. Yeh, Y. Zhang, High-entropy alloys: Fundamentals and applications, 2016. https://doi.org/10.1007/978-3-319-27013-5.

[3]   S.J. Sun, Y.Z. Tian, H.R. Lin, X.G. Dong, Y.H. Wang, Z.J. Zhang, Z.F. Zhang, Enhanced strength and ductility of bulk CoCrFeMnNi high entropy alloy having fully recrystallized ultrafine-grained structure, Mater. Des. 133 (2017). https://doi.org/10.1016/j.matdes.2017.07.054.

[4]   B. Gludovatz, A. Hohenwarter, D. Catoor, E.H. Chang, E.P. George, R.O. Ritchie, A fracture-resistant high-entropy alloy for cryogenic applications, Science (80-.). 345 (2014). https://doi.org/10.1126/science.1254581.

[5]   M.H. Chuang, M.H. Tsai, W.R. Wang, S.J. Lin, J.W. Yeh, Microstructure and wear behavior of AlxCo 1.5CrFeNi1.5Tiy high-entropy alloys, Acta Mater. 59 (2011).

https://doi.org/10.1016/j.actamat.2011.06.041.

[6] P. Koželj, S. Vrtnik, A. Jelen, M. Krnel, D. Gačnik, G. Dražić, A. Meden, M. Wencka, D. Jezeršek, J. Leskovec, S. Maiti, W. Steurer, J. Dolinšek, Discovery of a FeCoNiPdCu High-Entropy Alloy with Excellent Magnetic Softness, Adv. Eng. Mater. 21 (2019). https://doi.org/10.1002/adem.201801055.

[7] J.-W. Yeh, S.-K. Chen, S.-J. Lin, J.-Y. Gan, T.-S. Chin, T.-T. Shun, C.-H. Tsau, S.-Y. Chang, Nanostructured High-Entropy Alloys with Multiple Principal Elements: Novel Alloy Design Concepts and Outcomes, Adv. Eng. Mater. 6 (2004) 299–303. https://doi.org/10.1002/adem.200300567.

[8] B. Cantor, I.T.H. Chang, P. Knight, A.J.B. Vincent, Microstructural development in equiatomic multicomponent alloys, Mater. Sci. Eng. A. 375–377 (2004). https://doi.org/10.1016/j.msea.2003.10.257.

[9] D.B. Miracle, O.N. Senkov, A critical review of high entropy alloys and related concepts, Acta Mater. 122 (2017). https://doi.org/10.1016/j.actamat.2016.08.081.

[10] Y.J. Zhou, Y. Zhang, Y.L. Wang, G.L. Chen, Microstructure and compressive properties of multicomponent Alx(TiVCrMnFeCoNiCu)100-x high-entropy alloys, Mater. Sci. Eng. A. 454–455 (2007). https://doi.org/10.1016/j.msea.2006.11.049.

[11] B.S. Li, Y.P. Wang, M.X. Ren, C. Yang, H.Z. Fu, Effects of Mn, Ti and V on the microstructure and properties of AlCrFeCoNiCu high entropy alloy, Mater. Sci. Eng. A. 498 (2008). https://doi.org/10.1016/j.msea.2008.08.025.

[12] Y.L. Chen, Y.H. Hu, C.A. Hsieh, J.W. Yeh, S.K. Chen, Competition between elements during mechanical alloying in an octonary multi-principal-element alloy system, J. Alloys Compd. 481 (2009). https://doi.org/10.1016/j.jallcom.2009.03.087.

[13] S. Guo, C.T. Liu, Phase stability in high entropy alloys: Formation of solid-solution phase or amorphous phase, Prog. Nat. Sci. Mater. Int. 21 (2011). https://doi.org/10.1016/S1002-0071(12)60080-X.

[14] S. Guo, C. Ng, J. Lu, C.T. Liu, Effect of valence electron concentration on stability of fcc or bcc phase in high entropy alloys, in: J. Appl. Phys., 2011. https://doi.org/10.1063/1.3587228.

[15] A.K. Singh, A. Subramaniam, On the formation of disordered solid solutions in multi-component alloys, J. Alloys Compd. 587 (2014). https://doi.org/10.1016/j.jallcom.2013.10.133.

[16] X.F. Wang, Y. Zhang, Y. Qiao, G.L. Chen, Novel microstructure and properties of multicomponent CoCrCuFeNiTix alloys, Intermetallics. 15 (2007). https://doi.org/10.1016/j.intermet.2006.08.005.

[17] C.J. Tong, Y.L. Chen, S.K. Chen, J.W. Yeh, T.T. Shun, C.H. Tsau, S.J. Lin, S.Y. Chang, Microstructure characterization of AlxCoCrCuFeNi high-entropy alloy system with multiprincipal elements, Metall. Mater. Trans. A Phys. Metall. Mater. Sci. 36 (2005). https://doi.org/10.1007/s11661-005-0283-0.

[18] J. Wang, Y. Zhang, S.Z. Niu, W.Y. Wang, H.C. Kou, J.S. Li, S.Q. Wang, E. Beaugnon, Formation of a hexagonal closed-packed phase in Al0.5CoCrFeNi high entropy alloy, MRS Commun. 7 (2017). https://doi.org/10.1557/mrc.2017.109.

[19] B.S. Murty, S. Ranganathan, J.W. Yeh, P.P. Bhattacharjee, High-entropy alloys, 2019. https://doi.org/10.1016/C2017-0-03317-7.

[20] S. Syed Ghazi, K.R. Ravi, Phase-evolution in high entropy alloys: Role of synthesis route, Intermetallics. 73 (2016). https://doi.org/10.1016/j.intermet.2016.03.002.

[21] C.C. Koch, Nanocrystalline high-entropy alloys, J. Mater. Res. 32 (2017). https://doi.org/10.1557/jmr.2017.341.

[22] N.F. Shkodich, M. Spasova, M. Farle, D.Y. Kovalev, A.A. Nepapushev, K.V. Kuskov, Y.S. Vergunova, Y.B. Scheck, A.S. Rogachev, Structural evolution and magnetic properties of high-entropy CuCrFeTiNi alloys prepared by high-energy ball milling and spark plasma sintering, J. Alloys Compd. 816 (2020).

https://doi.org/10.1016/j.jallcom.2019.152611.

[23] S. Varalakshmi, M. Kamaraj, B.S. Murty, Synthesis and characterization of nanocrystalline AlFeTiCrZnCu high entropy solid solution by mechanical alloying, J. Alloys Compd. 460 (2008). https://doi.org/10.1016/j.jallcom.2007.05.104.

[24] N.F. Shkodich, A.S. Rogachev, S.G. Vadchenko, D.O. Moskovskikh, N. V. Sachkova, S. Rouvimov, A.S. Mukasyan, Bulk Cu-Cr nanocomposites by high-energy ball milling and spark plasma sintering, J. Alloys Compd. (2014). https://doi.org/10.1016/j.jallcom.2014.07.133.

[25] B.S. Murty, S. Ranganathan, Novel materials synthesis by mechanical alloying/milling, Int. Mater. Rev. 43 (1998). https://doi.org/10.1179/imr.1998.43.3.101.

[26] N. Shkodich, A. Sedegov, K. Kuskov, S. Busurin, Y. Scheck, S. Vadchenko, D. Moskovskikh, Refractory high-entropy hftatinbzr-based alloys by combined use of ball milling and spark plasma sintering: Effect of milling intensity, Metals (Basel). 10 (2020). https://doi.org/10.3390/met10091268.

[27] Z. An, H. Jia, Y. Wu, P.D. Rack, A.D. Patchen, Y. Liu, Y. Ren, N. Li, P.K. Liaw, Solid-solution CrCoCuFeNi high-entropy alloy thin films synthesized by sputter deposition, Mater. Res. Lett. 3 (2015). https://doi.org/10.1080/21663831.2015.1048904.

[28] M. Arfaoui, G. Radnóczi, V.K. Kis, Transformations in CrFeCoNiCu high entropy alloy thin films during in-situ annealing in TEM, Coatings. 10 (2020). https://doi.org/10.3390/coatings10010060.

[29] N. Park, I. Watanabe, D. Terada, Y. Yokoyama, P.K. Liaw, N. Tsuji, Recrystallization Behavior of CoCrCuFeNi High-Entropy Alloy, Metall. Mater. Trans. A Phys. Metall. Mater. Sci. 46 (2015). https://doi.org/10.1007/s11661-014-2594-5.

[30] C.M. Lin, H.L. Tsai, H.Y. Bor, Effect of aging treatment on microstructure and properties of high-entropy Cu0.5CoCrFeNi alloy, Intermetallics. 18 (2010). https://doi.org/10.1016/j.intermet.2010.03.030.

[31] H. Zheng, R. Chen, G. Qin, X. Li, Y. Su, H. Ding, J. Guo, H. Fu, Microstructure evolution, Cu segregation and tensile properties of CoCrFeNiCu high entropy alloy during directional solidification, J. Mater. Sci. Technol. 38 (2020). https://doi.org/10.1016/j.jmst.2019.08.019.

[32] V.K. Pandey, V. Shivam, B.N. Sarma, N.K. Mukhopadhyay, Phase evolution and thermal stability of mechanically alloyed CoCrCuFeNi high entropy alloy, Mater. Res. Express. 6 (2019). https://doi.org/10.1088/2053-1591/ab618f.

[33] S. Praveen, B.S. Murty, R.S. Kottada, Alloying behavior in multi-component AlCoCrCuFe and NiCoCrCuFe high entropy alloys, Mater. Sci. Eng. A. 534 (2012). https://doi.org/10.1016/j.msea.2011.11.044.

[34] S. Thangaraju, T.E. Bouzy, A. Hazotte, Phase Stability of a Mechanically Alloyed CoCrCuFeNi High Entropy Alloy, Adv. Eng. Mater. 19 (2017). https://doi.org/10.1002/adem.201700095.

[35] G.K. Williamson, W.H. Hall, X-ray line broadening from filed aluminium and wolfram, Acta Metall. 1 (1953). https://doi.org/10.1016/0001-6160(53)90006-6.

[36] S. Varalakshmi, M. Kamaraj, B.S. Murty, Formation and stability of equiatomic and nonequiatomic nanocrystalline CuNiCoZnAlTi high-entropy alloys by mechanical alloying, Metall. Mater. Trans. A Phys. Metall. Mater. Sci. 41 (2010). https://doi.org/10.1007/s11661-010-0344-x.